Morphodynamic Evolution of a Fringing Sandy Shoal From Tidal Levees to Sea Level Rise

Elmilady, H.; Van Der Wegen, M.; Roelvink, D.; van der Spek, A.

DOI
10.1029/2019JF005397

Publication date
2020

Document Version
Final published version

Published in
Journal of Geophysical Research: Earth Surface

Citation (APA)
Elmilady, H., Van Der Wegen, M., Roelvink, D., & van der Spek, A. (2020). Morphodynamic Evolution of a Fringing Sandy Shoal: From Tidal Levees to Sea Level Rise. *Journal of Geophysical Research: Earth Surface*, *125*(6), 1-21. Article e2019JF005397. https://doi.org/10.1029/2019JF005397

JGR Earth Surface

RESEARCH ARTICLE
10.1029/2019JF005397

Morphodynamic Evolution of a Fringing Sandy Shoal: From Tidal Levees to Sea Level Rise

H. Elmilady[1,2,3], M. van der Wegen[1,2], D. Roelvink[1,2,3], and A. van der Spek[2,4]

[1]IHE Delft Institute for Water Education, Delft, Netherlands, [2]Deltares, Delft, Netherlands, [3]Faculty of Civil Engineering and Geosciences, Delft University of Technology, Delft, Netherlands, [4]Faculty of Geosciences, Utrecht University, Utrecht, Netherlands

Key Points:
- At sandy shoals, most short-term morphodynamic activity occurs near the channel-shoal interface
- Variations in wind-wave forcing cause the formation of tidal levees
- Shoals accrete in response to sea level rise with a long (decades) bed-level adaptation lag eventually leading to intertidal area loss

Supporting Information:
- Supporting Information S1
- Movie S1
- Movie S2
- Movie S3

Correspondence to:
H. Elmilady,
h.elmilady@un-ihe.org

Citation:
Elmilady, H., van der Wegen, M., Roelvink, D., & van der Spek, A. (2020). Morphodynamic evolution of a fringing sandy shoal: From tidal levees to sea level rise. *Journal of Geophysical Research: Earth Surface*, *125*, e2019JF005397. https://doi.org/10.1029/2019JF005397

Received 3 OCT 2019
Accepted 4 MAY 2020

Abstract Intertidal shoals are vital components of estuaries. Tides, waves, and sediment supply shape the profile of estuarine shoals. Ensuring their sustainability requires an understanding of how such systems will react to sea level rise (SLR). In contrast to mudflats, sandy shoals have drawn limited attention in research. Inspired by a channel-shoal system in the Western Scheldt Estuary (Netherlands), this research investigates governing processes of the long-term morphodynamic evolution of intertidal estuarine sandy shoals across different timescales. We apply a high-resolution process-based numerical model (Delft3D) to generate a channel-shoal system in equilibrium and expose the equilibrium profile to variations in wave forcing and SLR. Combined tidal action and wave forcing initiate ridge formation at the seaward shoal edge, which slowly propagates landward until a linear equilibrium profile develops within 200 years. Model simulations in which forcing conditions have been varied to reproduce observations show that the bed is most dynamic near the channel-shoal interface. A decrease/increase in wave forcing causes the formation/erosion of small tidal levees at the shoal edge, which shows good resemblance to observed features. The profile recovers when regular wave forcing applies again. Sandy shoals accrete in response to SLR with a long (decades) bed-level adaptation lag eventually leading to intertidal area loss. This lag depends on the forcing conditions and is lowest near the channel and gradually increases landward. Adding mud makes the shoal more resilient to SLR. Our study suggests that processes near the channel-shoal interface are crucial to understanding the long-term morphodynamic development of sandy shoals.

Plain Language Summary Intertidal area is the coastal zone that undergoes a rhythm of wet-dry cycles under the influence of tidal action. Intertidal shoals are vital components of the estuarine environment. They have high ecological value but also help in reducing flood risk by wave attenuation. It is important to understand how these shoals will react to sea level rise in order to plan sustainable management strategies. We developed a high-resolution model to investigate the long-term evolution of an intertidal sandy channel-shoal system. The model describes tidal flow, wave action, and associated sediment transports and generates an intertidal sandy shoal in equilibrium. Changes in equilibrium forcing lead to morphodynamic adaptation. A drop in wave height causes the formation of small-scale tidal levees at the channel-shoal edge, which are also observed in reality. High wind-wave activity causes shoal erosion. Shoals accrete in response to imposing sea level rise, but the accretion rate is smaller than the sea level rise rate leading to the loss of intertidal area and increased inundation. Inclusion of mud makes the shoal more resilient to sea level rise. Our study suggests that processes near the channel-shoal edge are crucial to understanding the long-term morphodynamic evolution of sandy shoals.

1. Introduction

Intertidal shoals are a major component of many estuaries worldwide. During the tidal cycle, they undergo a rhythm of wet-dry cycles which develops a unique ecosystem that supports a diverse array of species, especially at vegetated zones (Lipcius et al., 2013). The intertidal area provides ecosystem services and accommodates commercial fisheries. It also plays a major role in erosion control and flood protection by wave attenuation (Narayan et al., 2017; Shepard et al., 2011).

Being the buffer zone between sea and land, the intertidal zone is subject to continuous pressures like urbanization, changing river flow regime and sediment supply, subsidence, and sea level rise (SLR). Anthropogenic influence may notably impact the estuarine morphology (e.g., Jaffe et al., 2007;

Luan et al., 2016; Ranasinghe et al., 2019) potentially leading to a notable degradation of the intertidal ecosystem and a continuous threat to associated ecosystem services.

Estuarine shoals may be considered as emergent features that evolve as a result of a fundamental instability of the morphodynamic system under tidal forcing. An initial bed-level perturbation triggers a positive morphodynamic feedback between currents and morphology leading to the emergence of large-scale channel-shoal patterns (Coeveld et al., 2003; Hibma et al., 2003; Schramkowski et al., 2002; Seminara & Tubino, 2001). Over a long timescale (centuries to millennia), the residual sediment transport diminishes and leads to a relatively stable channel-shoal morphology where braiding ebb and flood channels circumvent sandy shoals (Ahnert, 1960; Hibma, 2004; Leuven et al., 2016; van der Wegen et al., 2008; van der Wegen & Roelvink, 2008; van Veen et al., 2005). Confined estuarine plan forms govern the location and evolution of particular channel-shoal patterns (Dam et al., 2016; Leuven et al., 2018; van der Wegen & Roelvink, 2012).

Although the previous section suggests that shoal formation is primarily associated with tidal currents, waves play an important role when shoals become shallow and intertidal (e.g., Kohsiek et al., 1988). Observations and modeling studies suggest that tidal flats tend to evolve toward a morphologically steady-state maintained by a balance between sediment supply, wave action, and tidal forcing (Friedrichs, 2011; Friedrichs & Aubrey, 1996; Hu et al., 2015; Maan et al., 2015, 2018; Roberts et al., 2000; van der Wegen et al., 2017, 2019). Tidal forcing is usually associated with deposition while erosion tends to be associated with wind-wave activity (e.g., Allen & Duffy, 1998; Christie et al., 1999; Janssen-Stelder, 2000; Yang et al., 2003). Spatial gradients in hydrodynamic energy and suspended sediment concentrations (SSC) across the tidal flat impact the direction of sediment flux. Tidal currents cause highest bed stresses at the deeper (subtidal) flat section, driving a landward transport, while wind-waves cause highest stresses on the shallower (intertidal) flat section, driving a seaward transport (e.g., Friedrichs, 2011; Kohsiek et al., 1988; Ridderinkhof et al., 2000; Yang et al., 2003). Janssen-Stelder (2000) shows a landward directed tidally averaged suspended sediment flux across tidal flats in the Wadden Sea during calm wave conditions, which reverses to seaward as wave heights grew.

In addition to its erosional capacity, waves impact the sediment redistribution along the flat (Carniello et al., 2005; Houser & Hill, 2010; Zhou et al., 2015). Intertidal shoals can be mudflats, sand flats, or a mixture depending on the sediment supply and hydrodynamic conditions. They can be found in a free (no landward constrains) or a fringing form. Sand fractions exist at locations where wave action and strong tidal currents prevent fine sediment deposition while mud fractions exist at more sheltered low-energy embayments and fringes.

1.1. Modeling Intertidal Flats

Several morphodynamic modeling studies explored tidal evolution and equilibrium profiles for a muddy environment including wave impact. This “morphological equilibrium” is loosely defined in literature as a state at which tide-residual transport diminishes and limited morphological development occurs within a characteristic forcing time span (Friedrichs, 2011; Zhou et al., 2017). Friedrichs and Aubrey (1996) proposed a dynamic equilibrium theory with analytical solutions under the assumption of spatially constant maximum shear stress. Assuming a similar equilibrium concept, Hu et al. (2015) implemented the dynamic equilibrium theory while allowing for spatially and temporally varying bed shear stress.

Other studies implemented a process-based approach without underlying assumptions of equilibrium (e.g., Pritchard et al., 2002; Pritchard & Hogg, 2003). Roberts et al. (2000) and van der Wegen et al. (2017, 2019) showed modeled 1-D profiles similar to observed mudflat profiles; 2-D/3-D processed-based models provided skillful reproduction of observed morphodynamic developments in entire estuaries such as San Francisco Bay (Ganju et al., 2009; van der Wegen et al., 2011; Elmilady et al., 2019), Western Scheldt (Maan et al., 2018), and Yangtze Estuary (Guo, 2014; Luan et al., 2016, 2017).

However, process-based modeling studies covering sandy shoals only applied relatively coarse grids and excluded wave dynamics (e.g., Dam et al., 2016; Guo, 2014; Hibma, 2004; van der Wegen, 2013; van der Wegen & Roelvink, 2008, 2012) to reduce computational effort and model complexity. Braat et al. (2017) modeled waves in a sand-mud estuarine environment, albeit with a sand transport formulation (Engelund & Hansen, 1967) which models a total transport and exclude sand stirring by waves. The inclusion of

waves in sandy systems could be of high relevance, especially for the intertidal morphology. In addition, a relatively coarse grid could potentially disregard relevant subgrid (wave) dynamics and features.

1.2. Tidal Levees

An example of subgrid features is a tidal levee. Levees are small ridges formed by deposits that build up along the sides of a channel. Their formation is commonly pronounced in riverine and deltaic systems during flood events (Adams et al., 2004; Brierley et al., 1997) or along submarine fan system channels during high flow turbid events (Normark et al., 2002; Straub & Mohrig, 2008). In tidal environments, they can be found along creeks in salt marshes and mudflats (Perillo & Iribarne, 2003; Temmerman et al., 2005) or on the edge of channels and shoals in tidal basins and estuaries (Cleveringa, 2013). They often fall dry near low water before the surrounding shoal area and usually consist of coarser material than that found on locations further away from the channel edge. Unlike riverine levees, tidal levees have drawn limited attention in research.

Based on field observations of sand transport and morphological changes in intertidal areas (Eastern Scheldt estuary; The Wash, UK; Wadden Sea), Wang et al. (2018, pp. 194–197) developed a conceptual model for sandy tidal flat development over long timescales. They describe the flat evolution as the outcome of the opposing supply of suspended sand by the tide, predominantly at the shoal edge, and (re)suspension or erosion of the shoal surface sediments by waves. Formation of tidal levees has been observed during periods of mild wave conditions.

1.3. SLR

Tide gauge records show that the sea level has risen about 20 cm during the past century (Kemp et al., 2011). Currently, the SLR rate is 3.3 mm/year (NASA, 2019) with considerable global variations (Handleman, 2015). This rate is expected to accelerate toward the end of the 21st century (Church et al., 2013; Parris et al., 2012). It is unclear how estuaries will morphodynamically react to SLR in particular with respect to the fate of intertidal area. The estuarine resilience to SLR may strongly depend on local conditions of tides, waves, sediment supply, and local SLR rate.

Process-based models provide useful tools to explore the possible impact of SLR on estuarine morphodynamics. SLR impact studies include validated modeling hindcasts (Elmilady et al., 2019; Ganju & Schoellhamer, 2010; van der Wegen et al., 2017; Zhou et al., 2013) or more schematized settings systematically exploring governing processes (Best et al., 2018; Dissanayake et al., 2009; van der Wegen, 2013; van Maanen et al., 2013; Zhou et al., 2016). Rossington and Spearman (2009) and Van Goor et al. (2003) provide SLR studies applying an empirical approach (ASMITA), albeit that potential wave impact was not considered explicitly. A common finding of previous studies is that SLR leads to intertidal area accretion; however, the accretion rate is less than the SLR rate. A limited, linear rise in sea level may allow for an accretion rate equal to the SLR rate after an initial period of intertidal area loss (Van Goor et al., 2003).

1.4. Research Objective

This study aims to explore the mechanisms that drive the long-term morphodynamic evolution of sandy intertidal shoals across a range of timescales. This includes the mechanisms driving the formation of tidal levees and the impact of SLR. We hypothesize that a stable intertidal shoal morphology evolves from a balance between constant sediment supply, tidal action, and wave forcing and that changes in forcing lead to adaptation of this equilibrium profile that may recover when prevailing forcing is maintained again.

First, we focus on observed sandy shoal dynamics. We revisit field measurements carried out by Geomor team (1984) at the Galgeplaat shoal in the Eastern Scheldt Estuary (Figure 1). We then explore satellite imagery of sandy shoals in the Western Scheldt Estuary (WS, Figure 2) and LIDAR data at the Frisian Inlet in the Wadden Sea (Figure 3). Second, we apply a process-based model (Delft3D) that allows for a flexible application of processes across a range of scales. Using a schematized configuration inspired by conditions in the WS, we investigate sandy shoal evolution and perform a sensitivity analysis for different model parameters and varying forcing conditions including variations in wave forcing and SLR rate. Finally, we qualitatively compare model results with observations and literature in order to test the developed knowledge regarding shoal dynamics and tidal levees. SLR impact is compared to the findings of an empirical, more aggregated modeling approach (ASMITA).

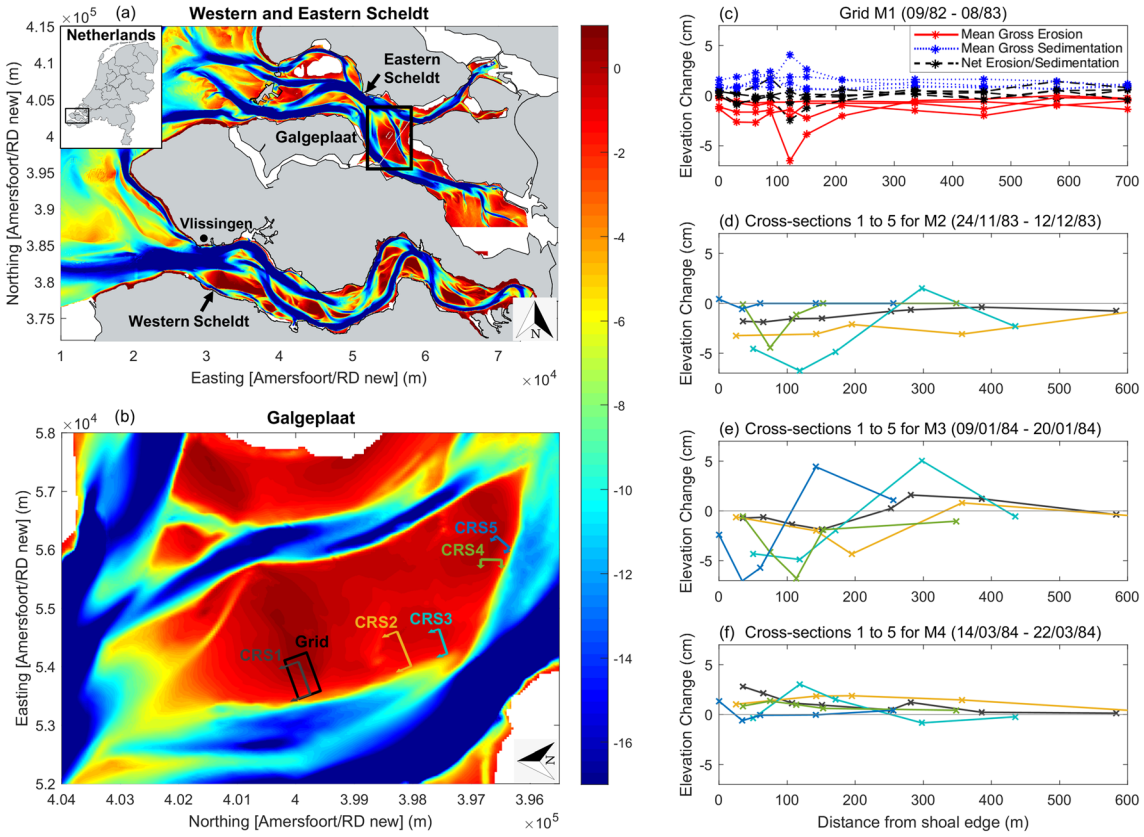

Figure 1. (a) Layout and bathymetry (m) of the Western and eastern Scheldt estuaries with the location of the Galgeplaat indicated. (b) The 1993 Galgeplaat bathymetry (m; reversed coordinates) showing the location of the 1982–1983 monitoring grid (black rectangle) along with the five cross sections (CRS1 to CRS5) monitored during 1983–1984 period. (c) Bed-level changes (cm) at four cross sections inside the monitoring grid during the 1-year monitoring period (M1) divided into the mean annual gross erosion (red) and sedimentation (blue) along with the net annual erosion/sedimentation (black). (d), (e), and (f) bed-level changes (cm) at CRS1 to CRS5 (colors correspond to cross sections in Figure 1b) during the monitoring periods of M2, M3, and M4, respectively. The figure was constructed by the digitization of Geomor team (1984) and van Vessem (1984a; 1984b). The bathymetric data (source: Rijkswaterstaat) are with respect to NAP (Dutch ordnance level).

2. Sandy Shoals Observations

The Eastern and Western Scheldt estuaries (Figure 1a) are located in the southwest of the Netherlands, while the Wadden Sea tidal basin is located in the north of the Netherlands (Figure 3). The morphology of these systems comprises a sandy system of deep channels and intertidal shoals which generally become muddier in more landward located regions. They are tide-dominated systems, the mean tidal range at the mouth of the WS (Vlissingen; Figure 1a) and the Frisian Inlet (Figure 3) is about 3.8 and 2 m, respectively. Shoals in the inner estuary are relatively sheltered from large offshore waves; wave attack is usually limited to small ($H_s < 0.25$ m) local wind-generated waves.

2.1. Eastern Scheldt

From 1982 to 1984, a unique pilot study was conducted with the aim of understanding the morphological evolution of the Eastern Scheldt shoals (Geomor team, 1984; Kohsiek et al., 1988; van Vessem, 1984a, 1984b). Since we managed to obtain only poor copies of these reports, we digitized the data and summarize their findings here. The study site is the Galgeplaat (Figure 1b) which is one of the largest (≈2.3 × 5.5 km) sandy intertidal shoals in the estuary. It becomes completely inundated during high tide while most of it is exposed during low tide.

Geomor team (1984) monitored bed-level changes on a 400 × 700 m grid of the Galgeplaat (Figure 1b, Black Rectangle) with four lateral monitoring cross sections (not shown on map) each with 11 monitoring points starting from the seaward shoal edge going landward. Geomor team (1984) and Kohsiek et al. (1988) noted

Figure 2. Google Earth satellite images showing small-scale levee formations at the channel-shoal interface in the WS. Note: Large and small images scales (bottom right) are 6 km and 200 m, respectively.

that the seaward shoal edge experienced most bed-level fluctuations compared to areas on top of the shoal. Shoal edge erosion mainly occurred under the influence of powerful wave action (wind speed > 5 Bft or ≈ 8 m/s, $H_s > 0.27$ m, $T_p \approx 3$ s). The increased wave action resulted in higher wave orbital velocities hence more

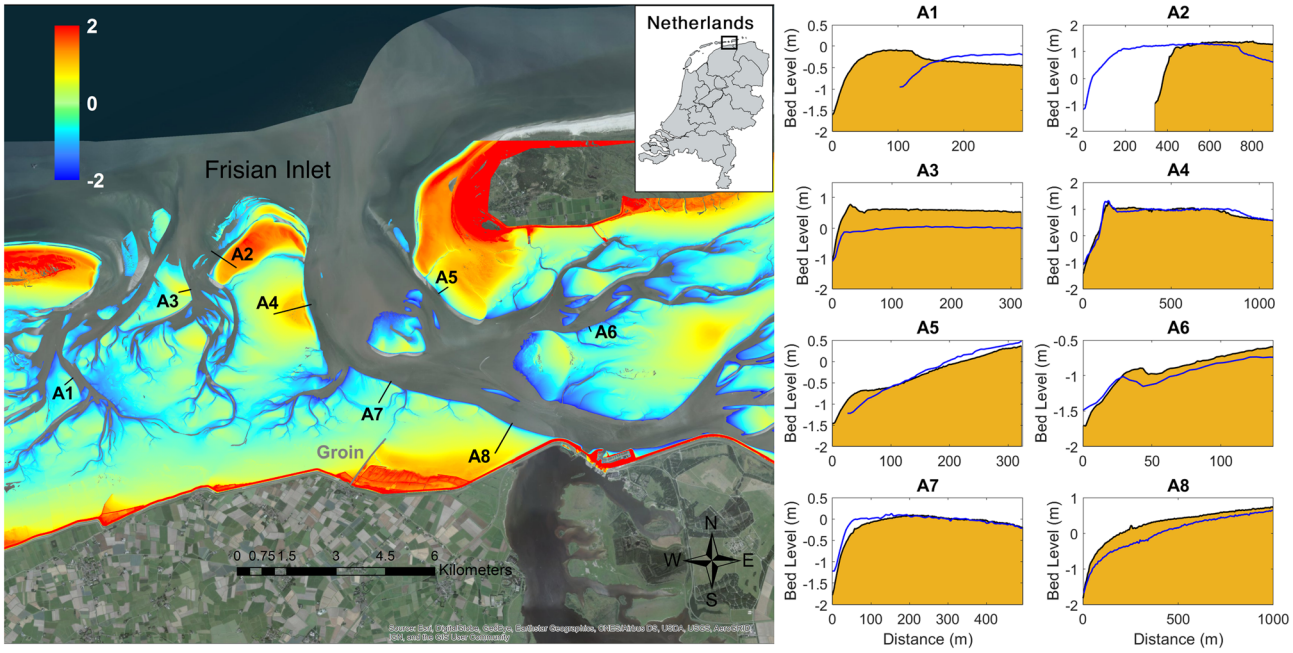

Figure 3. The left panel shows the 2018 bathymetry (m; reference NAP) of the intertidal zone at the Frisian inlet of the Wadden Sea obtained from LIDAR imagery (source: Rijkswaterstaat) along with the locations of eight cross sections (A1–A8). The right panel shows bed-level profiles for 2018 (black line and solid hatch) and 2012 (blue line). The left and right sides of a cross section are the seaward and landward sides, respectively.

resuspension. Combined with longshore and wind-driven currents, wave action increased the erosional transport capacity during stormy conditions. In contrast, during limited or no wave action (wind speed < 5 Bft or ≈ 8 m/s, H_s < 0.2 m, T_p ≈ 2 s), sedimentation processes dominated, especially during spring tides. Figure 1c shows that over the whole year (M1 monitoring period from September 1982 to August 1983), erosion and sedimentation were in the same order resulting in a relatively small net sedimentation/erosion.

From 1983 to 1984, bed levels were measured at five additional cross sections (CRS1 to CRS5, Figure 1b) at different points in time for durations ranging from 1 to 3 weeks (van Vessem, 1984a, 1984b). In this research, we present three monitoring periods (Figures 1d–1f), the two periods M2 and M3 represent intervals characterized with high wind-wave conditions while the period M4 represents an interval with mild wind-wave conditions. During M2 and M3, a clear erosional trend was observed, while during M4, the profile experienced net sedimentation. Similar to the 1-year monitoring period (M1), bed-level fluctuations mainly occurred at the shoal edge and decreased when going landward.

2.2. Remote Sensing at Western Scheldt and Wadden Sea

Relatively high elevation longitudinal ridge formations with dissecting drainage channels can be observed at the channel-shoal interface in sandy estuaries (e.g., Western Scheldt Estuary, Figure 2) and tidal basins (e.g., Wadden Sea, Figure 3). They can be visually identified as areas that emerge earlier during ebb tide than the surrounding shoal. Their width can be as small as 10 m which combined with their dynamic nature makes them hard to capture in large-scale bathymetric surveys. Figure 2 shows examples of levee formations spread along the WS. Cleveringa (2013) reports yearly measured high-resolution bed-level cross sections at several locations in the WS, some of which show levee formations at the channel-shoal interface.

LIDAR surveys during low tide are able to record the small-scale structures of the intertidal area. In this research, we present two LIDAR data sets (Figure 3) showing the Frisian Inlet of the Wadden Sea in 2012 and 2018 with 5 and 2 m spatial resolution, respectively.

Morphological ridge features resembling levees can be observed in a number of profiles at the shoal seaward edge. Their spatial scales can differ notably as their cross-sectional width ranged from 20 m (A6) up to 80 m (A1 2018). Tidal levees have a relatively dynamic nature, A4 and A6 show levees in both surveys, while A1, A3, and A5 show levees in just one survey. They can exist on a relatively flat profile (A1, A3, and A4) or on a sloping profile (A5 and A6). Also, in some cases (A2, A7, and A8), no visible levee formations were identified.

A7 and A8 are located on a sand-dominated shoal that resembles the schematized modeling configuration implemented in this study (section 3.1). The shoal is adjacent to a deep channel (15–20 m) on the north seaward side, and its configuration is relatively fringed. The adjacent polder blocks the flow from the eastern and southern direction and a groin blocks a portion of the flow from its open shallow western boundary. A7 experienced shoal edge erosion while the landward shoal side remained relatively constant. A8 shows an accreting profile with the highest accretion rates near the channel.

Within the presented map, there are several locations at which levees exist, but locations without levees are more common. The eight presented cross sections were selected from a large number of analyzed cross sections in order to show different morphodynamic behavior.

3. Numerical Model Setup

3.1. Model Setup and Forcing

We implemented a small-scale idealized 2DH modeling configuration that represents a fringing shoal in an estuarine channel-shoal system (Figure 4). This idealized approach allows for reducing the system's complexity. The setup is inspired by fringing shoals found along the edges of the WS (e.g., Maan et al., 2018). The initial bathymetry comprises a flat submerged 850 m wide shoal (−3 m MSL) adjacent to a 150 m wide channel (−15 m MSL). The model domain is covered by a 2-D horizontal fine resolution rectangular grid (20 × 30 m). We apply the Delft3D (D3D) process-based numerical model (Deltares, 2017; Lesser et al., 2004). Delft3D-FLOW computes the flow by solving the two-dimensional shallow water equations at a high spatial (20 × 30 m) and temporal (12 s) resolution (supporting information Text S1).

The only open model boundaries are at the channel, the northern, southern, and seaward boundary (black lines; Figure 4a). The seaward boundary is specified with a semi-diurnal, 1.75 m amplitude M_2 water level.

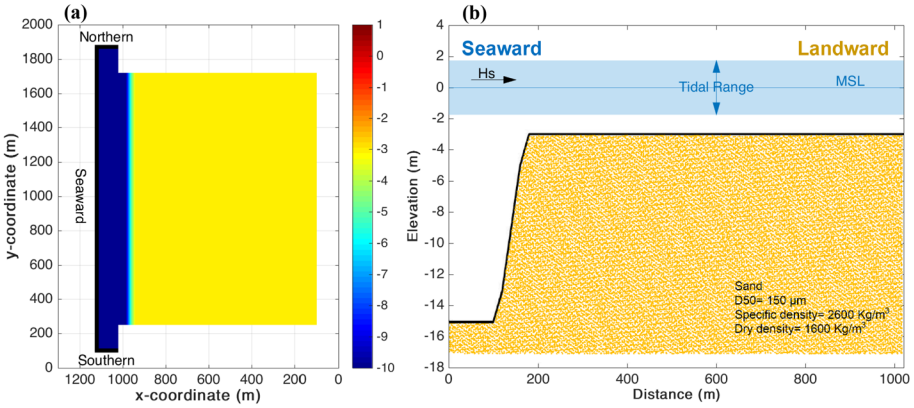

Figure 4. Model configuration and initial bathymetry (a) plan view with the location of the three open model boundaries (black lines) and (b) cross-sectional profile indicating the seaward and landward side along with the MSL, tidal range, wave direction, and initial sediment thickness and properties.

The northern and southern boundaries are Neumann water level gradient boundaries specified with a phase difference based on the tidal wave propagation in the channel. Equilibrium sediment concentrations at the boundaries were applied. A Thatcher-Harleman relaxation time lag of 120 min was set at the boundaries to avoid SSC discontinuities during the turning of tides (Thatcher & Harleman, 1972). We applied the "coastal boundary" option to allow non-perpendicular flow across the boundaries (Deltares, 2017).

3.2. Wave Model

Wave heights (H_s) and orbital velocities are computed using the "roller model" (Deltares, 2017, appendix B.15; J. A. Roelvink, 1993) which is coupled with Delft3D-FLOW through online coupling that includes wave-current interactions (wave-induced forcing included in the momentum equations). The roller model is used to simulate small ($H_s = 0.2$ m), short waves ($T_p = 3$ s) propagating from the seaward boundary toward the shoal (perpendicular to the shoal; Figure 4b). It incorporates a short wave energy balance equation in which friction and wave breaking are the dissipation mechanisms. Short wave energy dissipation due to wave breaking acts as the source term for a roller energy balance equation which delays the momentum release from wave breaking. Each time-step (12 s), the FLOW module computes (e.g., water level, velocities, and bed shear stress), and the roller model solves the wave energy propagation and dissipation across the shoal in order to evaluate the wave heights and its associated wave-induced shear stress. The Fredsoe wave-current interaction model (Fredsøe, 1984) is used to compute the maximum shear stress (τ_{max}, used for sediment computations) based on the combined flow (τ_c) and wave (τ_w) shear stress. A more detailed description of the roller model is provided in the supporting information (Text S2).

3.3. Sediment Transport and Morphodynamics

Suspended sediment transport is calculated in D3D by an advection-diffusion solver which includes a sink and source term and is based on the local and time-varying velocities and water levels. The Van Rijn (1993) formulations are used to compute the sandy sediment transport for the combined effect of waves and currents for both bed and suspended load transport (Text S3 provides more detailed information on the transport formulation).

We applied a noncohesive sediment fraction with a D_{50} of 150 μm, a sediment density of 2,650 kg/m^3 and a dry bed density of 1,600 kg/m^3. The minimum depth for sediment computations was set to 0.15 m. To account for bed slope effects, the transverse and streamwise bed gradient factors AlfaBn and AlfaBs were set as 20 and 1, respectively. The available sediment layer was set to −17 m MSL as initial runs showed a gradually continuous channel deepening. Instead of fixing the channel bed, this approach allows for the free development of the shoal along with limiting channel deepening.

Each time step (12 s), the MOR module in Delft3D-FLOW uses the combined hydrodynamics (FLOW + WAVE) to compute the sediment transport rates. Bed-level changes are calculated based on the divergence of the sediment transport field. Following that, bed-level changes are multiplied by a morphological acceleration factor (MF) to enhance morphological developments (Roelvink, 2006). This loop is

repeated for the next time-step using the updated bed levels. A MF of 100 was implemented for the base-case model based on a sensitivity analysis which showed minimal bed-level differences compared to a MF of 25 (Figure S1; supporting information of section 4.3). Using this approach, modeling 4 years of hydrodynamics with a MF of 100 is equivalent to 400 years of morphodynamic development. This approach has been widely applied in various long-term morphological studies (Elmilady et al., 2019; Dam et al., 2016; Ganju & Schoellhamer, 2010; Guo et al., 2015). The presented model takes about 2 days to simulate four hydrodynamic years on a 4-core computer.

4. Model Results

4.1. Development Toward Equilibrium

The initial bathymetry was subjected to constant tidal and wave forcing. The profile development starts first by a ridge formation near the channel which gradually grows horizontally landward and accretes vertically (Figure 5). The morphological development is rapid at the beginning but slows down over time. Morphological changes after a long time period (>200 years) are negligible. A 400 year simulation period was chosen to ensure equilibrium is achieved in all sensitivity simulations.

The initial bathymetry does not impact the equilibrium profile, but it affects the timescale at which equilibrium is achieved. The equilibrium bathymetry is slightly asymmetric along the *y*-axis due to a tide-residual, counter-clockwise wake flow on the shoal generated by the tide propagating from north to south. Also, higher flood velocities in the channel at the north leads to slightly higher SSC (sediment supply) during flood tide compared to southern locations. Since bed-level variations across the flat width are limited, all the cross-sectional plots and profiles presented throughout this research (e.g., Figure 5b) are a width-average of the 2-D model. The small bed-level irregularity at the landward most location is due to the assumption of a closed boundary which blocks the wave energy propagation leading to an abrupt drop in the wave group velocity and a local, small increase in wave height at the last cell (see Figure 6).

4.2. Intratidal Dynamics

We inspected the profile development during a tidal cycle (TCini) at an early stage of the simulation when the profile development is rapid. A MF of 200 is used to make bed-level changes more visible. TCini starts and ends at high water (Figure 6). The tidal wave is an almost standing wave. The phase lag between water levels and velocities is about 1 hr while the lag is about 0.5 hr longer on the shoal than in the channel. Movie S1 shows an animation of Figure 6 with higher temporal resolution.

The initial profile shows a ridge located at the shoal seaward side. In the vicinity of low water (t = 6 hr, Figures 6g and 6h), the shallow water depth over the ridge leads to high wave orbital velocities and wave energy dissipation due to bottom friction and breaking. The high wave-induced shear stress causes resuspension and creates a local SSC peak which combined with the flow drives suspended sediment transport. A landward directed suspended transport occurs at the landward section of the ridge which is slightly enhanced by a cross-shore wave-induced current. Whereas, a seaward directed transport occurs at the seaward shoal/ridge edge. In addition to the flow-induced transport, there is a wave-induced suspended transport component (included in Figure 6 within the bed load as described in supporting information Text S3) due to wave asymmetry effects. This component acts along the direction of the wave attack (landward). Both mechanisms cause erosion of the ridge top. A portion of this sediment is transported from the shoal toward the channel while the rest is redistributed landward resulting in the landward ridge growth.

As the water level rises and during maximum flood (t = 10 hr), the high flow velocities elevate the SSC in the channel which results in landward suspended sediment transport from the channel toward the ridge (Figures 6k and 6l). This mechanism causes deposition on top of the ridge which restores the previously eroded sediment and increases the ridge elevation slightly.

The sediment balance of the shoal can be simplified as tide-induced sediment input from the channel to the shoal edge counteracted by wave-induced erosion. During the initial stages of the profile development, tide-induced deposition is higher than wave-induced erosion due to the low shoal profile. The net sediment input to the shoal gets redistributed landward resulting in horizontal landward ridge growth along with slight vertical accretion as seen when comparing the initial bed-level profile (dotted black) to the profile at the end of the tidal cycle (solid black) in Figures 6m and 6n. This cycle repeats and the ridge continues

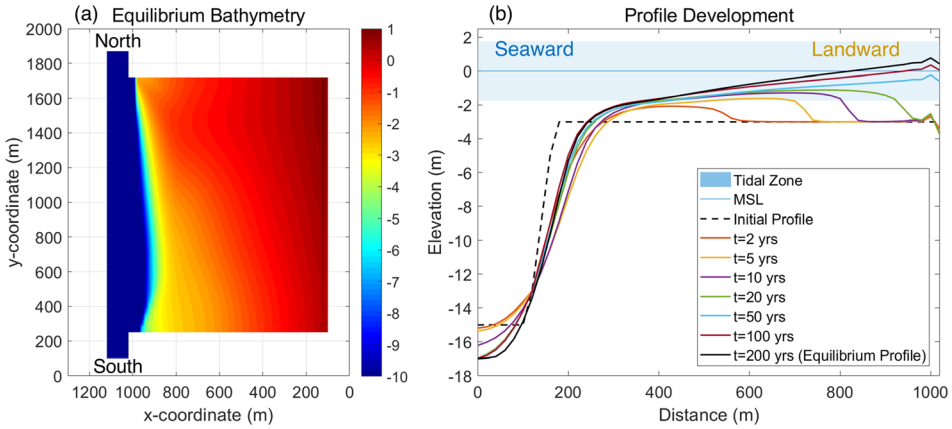

Figure 5. Modeled (a) equilibrium bathymetry after 200 years and (b) cross sectionally averaged bed-level profile showing the profile evolution over time toward an equilibrium state.

to move landward and increase in height. The horizontal landward ridge motion is rapid at the beginning of the evolution and slows down notably with time (Figure 5b) because sediment supplied from the channel needs to be transported over a longer distance. After the ridge reaches the landward boundary, the net landward transport accretes the profile which continues until a linear tidally averaged steady-state profile develops. Similar to the horizontal ridge growth, the vertical accretion rate decreases with time.

With the increase in profile elevation, the wave-induced shear stress increases resulting in higher wave-induced erosion. An equilibrium shoal profile is achieved when the tide-induced sediment supply from the channel to the shoal edge is balanced by a seaward sediment transport by wave-induced erosion. Figure 7a shows the tidally averaged flow ($\overline{\tau}_c$), wave ($\overline{\tau}_w$), and maximum ($\overline{\tau}_{max}$) shear stresses for tidal cycle TCini (at an early development stage) and TCeq (at equilibrium). The shear stress distribution for TCeq shows good resemblance with observations and modeling results presented by Maan et al. (2018) for a similar fringed shoal setting in the WS.

There is a limited difference in $\overline{\tau}_c$ between TCini and TCeq, while $\overline{\tau}_w$ and $\overline{\tau}_{max}$ increase notably over the equilibrium profile (Figure 7a) due to a higher elevation profile. For TCeq, the high $\overline{\tau}_{max}$ at the seaward shoal edge ($x \approx 200$–400 m) is due to both high $\overline{\tau}_c$ and $\overline{\tau}_w$. Flow velocities are higher than landward locations, also it is subjected to wave attack for a long period within the tidal cycle. Figure 7b shows the time-varying τ_w during tidal cycle TCeq. Wave shoaling occurs across the shoal which creates a positive landward τ_w gradient with a peak near the landward extent of the wet section followed by a sudden drop if wave breaking occurs. At low water ($t = 6$ hr), wave influence is confined to the shoal edge causing a high narrow local peak.

4.3. Sensitivity Analysis

A sensitivity analysis was performed using different forcing conditions (Figure 8) and model parameters (Figure S1 in the supporting information). Please refer to Table S1 in the supporting information for a full list of sensitivity runs. Exclusion of waves limits the suspension of sediments deposited at the shoal edge leading to the development of a pronounced high ridge (Figure 8a) and limited landward transport. A higher H_s steepens the profile with lower bed levels at the seaward shoal edge (Figure 8a). The H_s increase results in an increase in τ_w causing higher SSC over the developing ridge and more ridge top erosion along with higher transport rates. The landward section gets shallower due to larger landward sediment transport while higher τ_w at the shoal edge lowers its elevation. Also, the profile reaches equilibrium faster than that for milder wave conditions.

As the wave period (T_p) increases the profile gets steeper (Figure 8b). However, unlike the H_s increase, this increase is only due to higher bed levels at the landward edge while the seaward edge remains relatively constant. The reason is that the increase in T_p contributes to an enhanced wave asymmetry effect inducing landward suspended transport. However, it does not significantly impact τ_w on the developing ridge. Also, a larger T_p results in faster profile development.

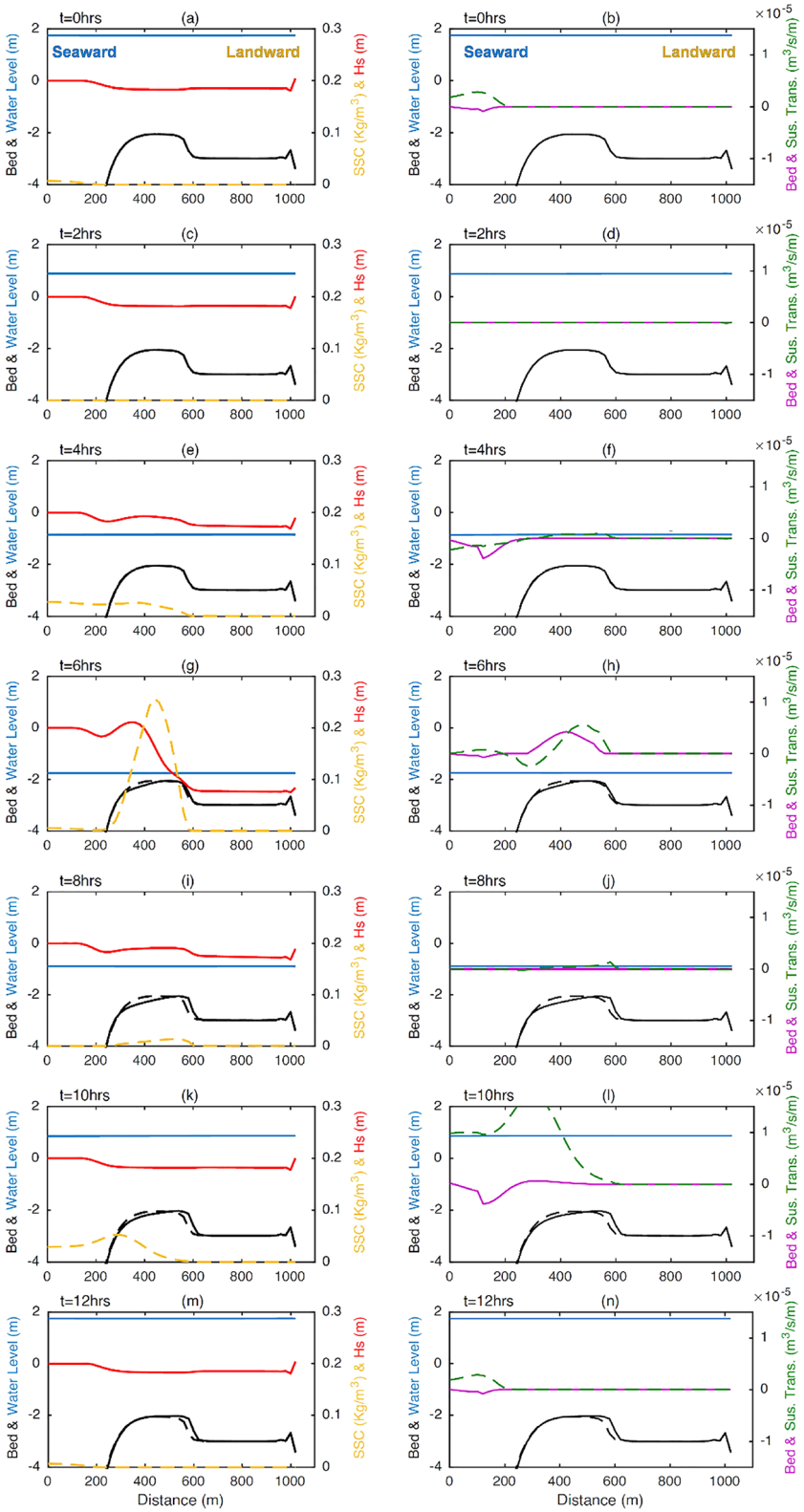

Figure 6. Cross-sectional profile showing the initial (t = 0 hr, dashed black) and time-varying (black) bed level, water level (blue), H_s (red), SSC (yellow), bed (magenta), and suspended (green) transport during tidal cycle TCini. Positive and negative transport are landward and seaward directed, respectively.

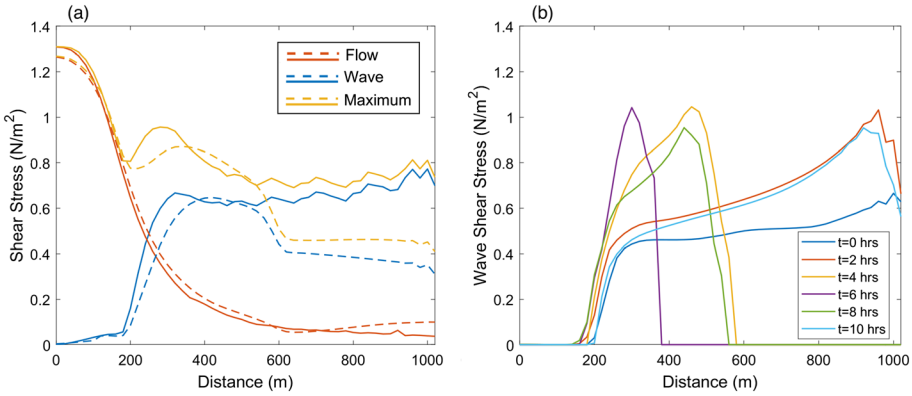

Figure 7. Modeled (a) flow ($\overline{\tau}_c$), wave ($\overline{\tau}_w$), and maximum ($\overline{\tau}_{max}$) tidally averaged shear stresses for tidal cycle TCini (dotted) and TCeq (continuous) and (b) wave-induced shear stress (τ_w) during tidal cycle TCeq. Note: For simplicity purposes, τ_w is roughly estimated by the difference between τ_{max} and τ_c.

The base-case applied a tidal range (dH) of 3.5 m to simulate a meso-tidal environment. Changing the tidal range alters the tidal velocities and the equilibrium concentrations at the boundary. Increasing dH shows a corresponding increase in the equilibrium profile elevation and a milder profile slope (Figure 8b). Larger dH results in higher channel flow velocities hence elevated channel SSC and a corresponding enhanced sediment supply toward the shoal.

Implementing finer (125 μm) and coarser (175 μm) sand fractions than the base-case ($D_{50} = 150$ μm) showed that coarser fractions result in steeper equilibrium profiles with a shallower landward shoal edge (Figure 8c) which provides a good agreement with observed trends in beaches.

In most sandy estuaries, fine mud fractions are present along sand in sheltered low-energy areas (e.g., Houser & Hill, 2010). We thus also explored the impact of a sand-mud mixture by starting from an initial sandy bed ($D_{50} = 150$ μm) and adding a relatively low mud concentration (25 mg/L) at the boundary. The Partheniades Krone formulations (Partheniades, 1965; see supporting information Text S3) are used for mud transport, with a critical erosion shear stress ($\tau_{c,e}$) of 0.2 N/m^2, an erosion parameter (M) of 2.5×10^{-4}, and a settling velocity (w_s) of 0.25 mm/s. For simplicity purposes, we do not account for sand-mud interactions. Figure 8c shows that the mixture equilibrium profile is steeper due to higher elevations at the landward edge. The relatively calm hydrodynamic conditions at the landward locations enhance mud deposition resulting in a muddier shoal than that at seaward locations. Also, the mixture profile reaches equilibrium faster than the base-case sand profile. This trend provides good agreement with previous studies (Maan et al., 2018; van der Wegen et al., (2017, 2019). In our model, this is attributed to the combined effect of a larger sediment supply and, more importantly, to the ability of mud fractions to remain in suspension for a longer time than sand so that landward locations are reached faster.

5. Forcing Variations

The equilibrium profiles presented in section 4 develop under constant forcing. However, in nature, external forcing conditions can vary continuously on a short (e.g., wind-waves) or long-term basis (e.g., SLR) which leaves the morphology out of equilibrium. In this section, we inspect the morphological response of the base-case equilibrium profile to forcing variations.

5.1. Wave Conditions

The base-case equilibrium profile was subjected to an increase and a decrease in wave height for six morphological months. Figure 9 shows that an increase in H_s results in a steeper profile with erosion at the seaward edge along with slight deposition at the landward limit. In contrast, the profile at the shoal seaward edge accretes in response to a decreased wave height, forming a small tidal levee with negligible bed-level changes more landward. The profile is in the process of adjusting toward a new equilibrium state with a milder slope and higher bed levels at the seaward shoal edge. In case of high elevation levees, drainage channels dissecting the levee start forming. Profile recovery after restoring the original forcing took somewhat longer than the perturbation duration.

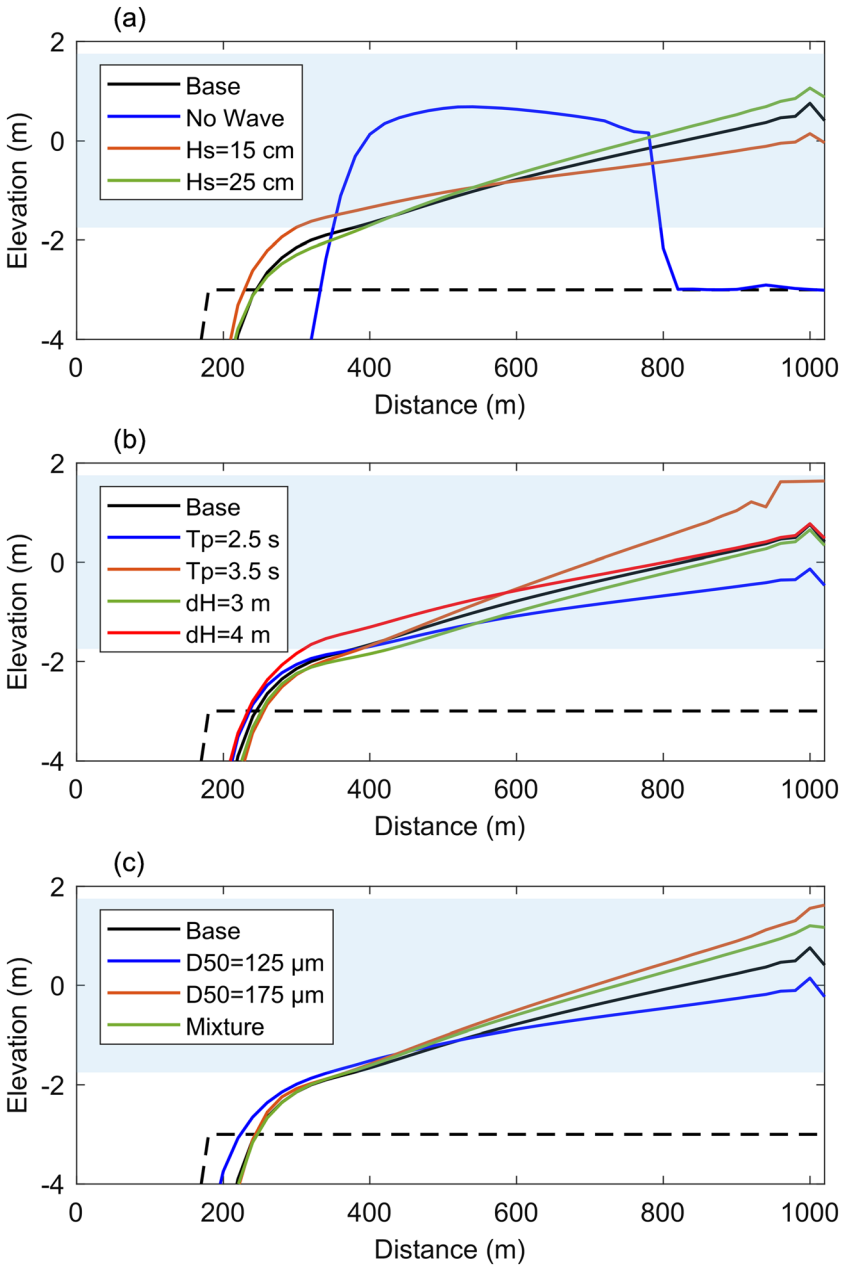

Figure 8. Sensitivity analysis showing the equilibrium profiles corresponding to different forcing conditions. The light blue shading indicates the base-case tidal difference, and the dashed black line indicates the initial profile.

The profile response to 12 hr (MF = 1) stormy wave conditions ($H_s \geq 1$ m, and $T_p = 6$ s) was similar to the response to the increased wave action but with a higher magnitude. Notable erosion occurred at the seaward shoal edge. The largest portion of the eroded sediment was transported seaward out of the model domain while a smaller portion got deposited landward on the shoal. Following the storm, the profile starts recovering rapidly. The largest part recovers within ≈2 years after the storm, although some small differences from the original equilibrium profile remain after 10 years. Please refer to supporting information Figure S2 for the impact of stormy conditions and recovery.

5.2. SLR

We imposed SLR on the equilibrium profile for 100 years with year 2000 as a starting point. The rise was prescribed as an increase in the mean sea level (MSL) based on a sinusoidal function and as a linear rise.

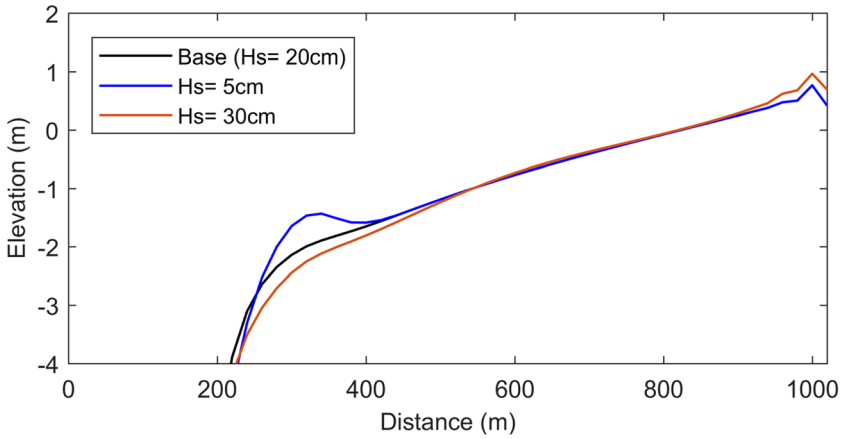

Figure 9. Cross-sectional bed-level profile after six morphological month wave forcing change.

Following that, we assume an abrupt stop of SLR for the following 200 years (2100–2300). This assumption allows for investigating the recovery from SLR.

When the SLRs based on a sinusoidal function (rising from the minimum to the intercept) during the first 100 years, the profile accretes in response (Figure 10). The larger water depth decreases the wave-induced shear stress allowing the profile to heighten. The accretion is largest near the channel and gradually extends landward. Due to inertial effects, a phase lag (decades) exists between SLR and the bed-level response. This lag increases over time with the increasing SLR rate. The lag is smallest near the channel and increases landward leading to a milder profile slope. Similar to tidal levee formation (section 5.1), the disturbance propagates from the shoal edge toward the landward limit (see Movie S2 for an animation of Figure 10).

Extending the simulations for 200 years with constant MSL showed a continued profile accretion till the profile reaches a new equilibrium state approximately equal to the old equilibrium profile plus the SLR magnitude. The recovery can range from decades to centuries based on the system's forcing conditions and the shoal dimensions. Seaward locations recover faster than landward locations. By 2300, the accretion was spatially uniform and the profile restored its initial 2000 slope. However, the profile remained about 3 cm deeper compared to MSL. A probable explanation is that the channel was maintained at the original depth so that tidal velocities decreased in a deeper channel leading to lower prevailing SSC at the channel edge.

Figures 11a and 11b show that for all simulations, by 2100, SLR resulted in a loss of intertidal area along with increased inundation (ratio between inundation duration and tidal period). Depending on the wave forcing, the intertidal area decline ranged from about 7% to 60%, and the inundation increased by about 8% to 15%. The initial profile at Year 2000 played an important role in determining the intertidal area resilience. The higher the initial elevation and the lower initial inundation, the less the intertidal area decrease was. A 14% increase to the initially high inundation (≈74%) of $H_s = 0.1$ m resulted in a notably larger intertidal area loss compared to a 10% increase to the initially lower inundation (≈57.5%) of the base-case ($H_s = 0.2$ m). Simulations with higher wave action experienced less intertidal area loss. The higher wave energy leads to an increase in sediment resuspension and transport rates which accelerates SLR adaptation.

Increased SLR rate results in an increased inundation and intertidal area decline (Figures 11c and 11d). This impact is nonlinear; the loss created by the 1.5 m scenario is not triple of that for the 0.5 m. In reality, this nonlinearity is expected to be more pronounced due to large-scale changes such as sediment supply, salinity, tidal prism, and tidal asymmetry.

We implemented a linear rise of a constant 10 mm/year (Figures 12a and 12b) leading to a rise in MSL after 100 years equal to the sinusoidal SLR. The reason to explore this is that SLR at the Dutch coast has been linear to date and no SLR rate increase has been observed (Vermeersen et al., 2018). This may be an exceptional but temporal trend due to specific local (northwestern Europe) conditions of SLR dynamics.

The linear 2100 profile experienced larger accretion at all points compared to the sinusoidal rise, with the difference increasing going landward. This resulted in a steeper profile along with a slight decrease in

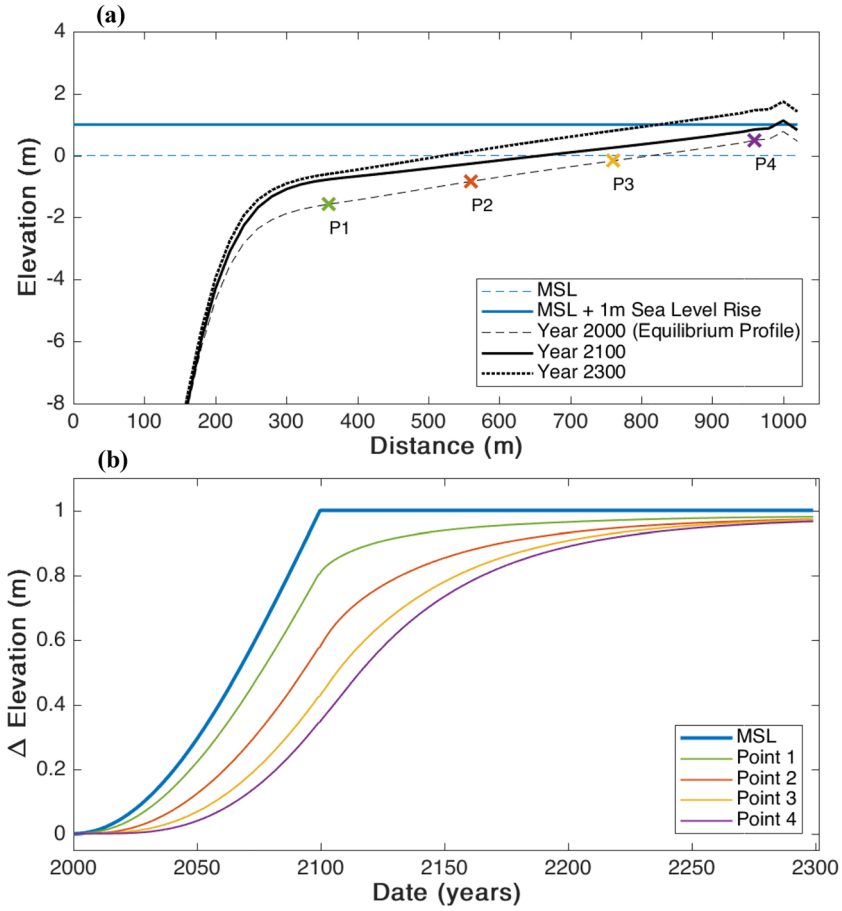

Figure 10. The top panel shows the forecasted bed levels at Years 2100 and 2300 under 1 m SLR scenario starting from the 2000 equilibrium profile and 0 m MSL. The bottom panel tracks the SLR and bed-level changes overtime at 4 points on the shoal.

intertidal area loss and inundation. The accretion is also largest near the channel edge and follows, with increasing lag the SLR. Fastest adaptation was at locations closer to the channel edge. After 100 years, the accretion rates at all locations are approximately similar, suggesting that the profile shape developed by then does not notably change. However, the 2100 rate (about 8.5 mm/year) is somewhat smaller than the SLR rate (10 mm/year). Extending the linear SLR toward 2200 (see supporting information Figure S3), showed that by 2200, the rates at all points approximately match the SLR rate. This suggests that the profile reached a new deeper, milder slope, equilibrium state that follows SLR at the same rate with a constant "overdepth."

We also imposed a sinusoidal SLR to the sand-mud mixture equilibrium profile presented in Figure 8c. The mixture simulation showed larger accretion in response to SLR, especially at landward locations (Figures 12c and 12d). The seaward most point (P1) experienced negligible differences as high shear stresses at seaward locations limit mud deposition. Mud fractions are able to remain in suspension for a longer period and reach calm landward locations faster than sand. This suggests that sandy-mud shoals are more resilient against SLR but will become muddier in case of SLR.

6. Discussion

6.1. Observed and Modeled Trends

Monitoring technics of intertidal shoals have notably improved in recent years. However, it is still hard to find a long-term data set of bed-level changes, waves, and currents with a high spatial and temporal resolution. This limits the possibility of performing a quantitative comparison between long-term model results

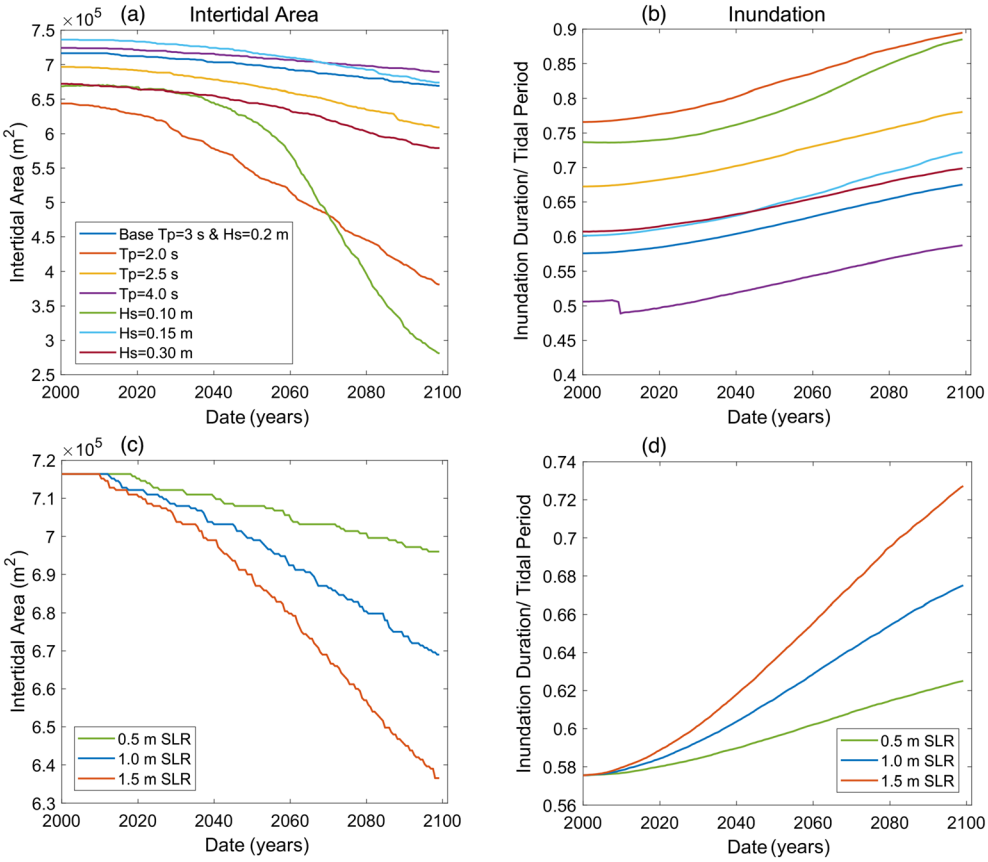

Figure 11. Modeled development of intertidal area (m^2) and its inundation over time for (a) and (b) different forcing conditions and (c) and (d) different SLR scenarios.

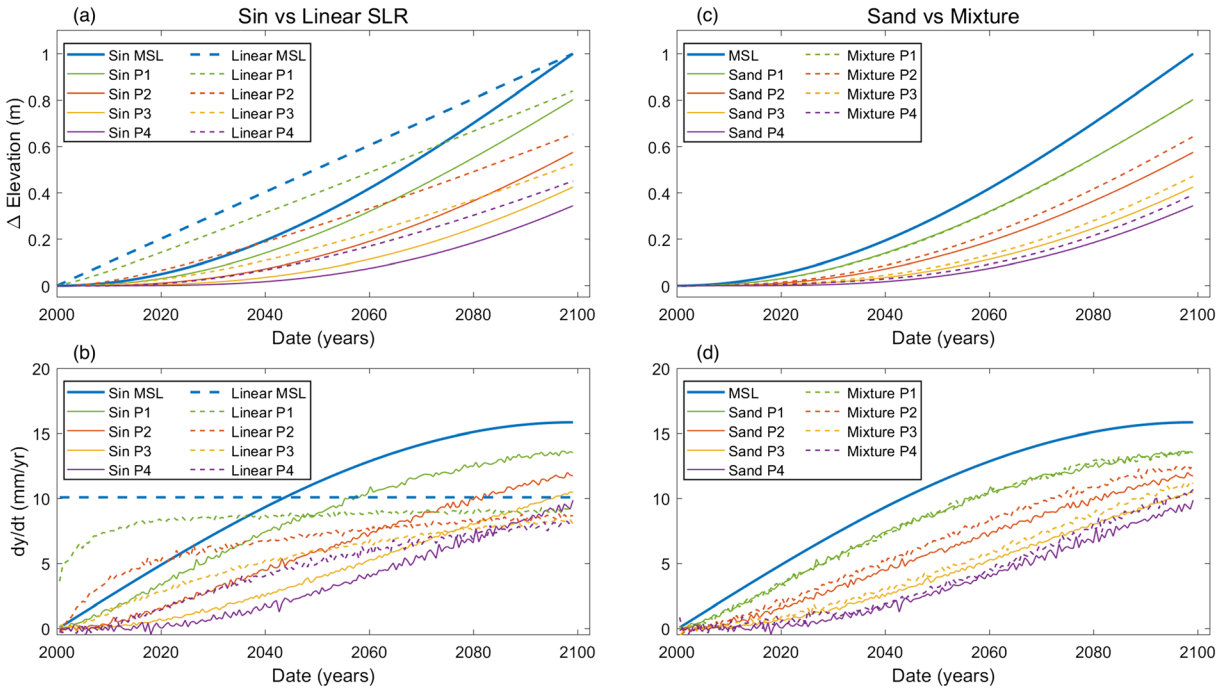

Figure 12. The top panels show SLR and bed-level changes at 4 points on the shoal (see Figure 10). The bottom panels show the rates.

and observations. In this section, we discuss our modeling approach and results in relation to the literature (section 1) and limited observations (section 2).

6.1.1. Shoal Dynamics

Shoals evolve over time toward a state of decreased morphological activity (e.g., Friedrichs, 2011; Maan et al., 2015, 2018). However, they tend to maintain a short-term, dynamic nature which can be mainly correlated to wind-wave activity. During calm conditions, shoals experience a net landward transport leading to shoal accretion while during high wave conditions a net seaward transport exists leading to shoal erosion (e.g., Allen & Duffy, 1998; Janssen-Stelder, 2000; Ridderinkhof et al., 2000; Wang et al., 2018). The seaward shoal section experiences more bed dynamics than landward locations (e.g., de Vet, 2020; Geomor team, 1984; Houser & Hill, 2010; Kohsiek et al., 1988).

Our modeling approach is based on the morphological equilibrium concept. Similar to previous modeling studies (Maan et al., 2018; Roberts et al., 2000; van der Wegen et al., 2017, 2019), the shoal evolve over time toward a state of reduced tide-residual sediment transport maintained by a balance between sediment supply, tidal forcing, and wave action. This state might imply the loss of shoal dynamics. However, the system dynamics are still maintained on the intratidal timescale. Despite being in an equilibrium state, the profile experiences intratidal bed-level changes which are largest at the shoal seaward edge ($x \approx 200$–400 m; see Movie S3 in the supporting information). The higher maximum shear stresses at this area (Figure 7a) enhances resuspension and makes it more dynamic compared to landward locations.

The shoal dynamics are also reflected in the modeled morphological response to forcing variations. Changes in equilibrium forcing impact the sediment balance leading to shoal evolution. A morphological disturbance starts at the shoal edge and propagates landward with time. Over the short timescale (days to month), the disturbance is somehow limited to the shoal seaward section. A long-term (century) forcing change such as SLR has a larger spatial-scale (whole shoal) impact with higher accretion again at seaward locations. Restoration of original forcing showed the profile recovery with associated timescales. Shoals are thus quite resilient systems that are able to adapt to and are not fundamentally changed by forcing variations.

Observations confirm this resilient nature, Geomor team (1984; Figure 1) show that during a monitoring year, the Galgeplaat experienced both periods of erosion and deposition with a relatively small net effect. Variations in the wind-wave climate were the main driver for the bed-level changes which were highest at the shoal seaward section. de Vet (2020) and Zhu et al. (2017) show that, in most instances, intertidal flats were able to recover from storm events. Van der Wegen et al. (2019) highlight that this resilience also holds for mudflats in response to seasonal forcing changes. Similar to the Galgeplaat, the largest morphological activity occurred at the mudflat edge and channel slope while it notably decreased toward the landward section.

6.1.2. Tidal Levees

In nature, shoals usually appear to be quite stable in the sense that, over some characteristic period of natural forcing, they do not experience notable morphological changes that fundamentally alter their structure. However, we do not expect that shoals reach an equilibrium state in the strict sense due to the continuous forcing changes which operate at multiple timescales and the inertia involved in the profile adaptation (Zhou et al., 2017).

A close investigation of measured intertidal shoal profiles and satellite imagery over the short timescale (years) in the WS (e.g., Figure 2; Cleveringa, 2013) and Wadden Sea (e.g., Figure 3) showed tidal levee formations at the shoal seaward edge (channel-shoal interface). Such features have different spatial scales (dimensions) and relatively dynamic nature (short-lived features). They exist on different profile shapes, while some profiles do not show such formations.

We hypothesized that their evolution is an essential part of the shoal evolution. Model results show that sustained durations of forcing conditions favoring deposition (e.g., drop of wave action) resulted in a net landward transport causing levee formation at the profile seaward edge. On the other hand, an increase in wave action resulted in a net seaward transport causing the destruction of such features along with shoal edge erosion.

Clear examples of tidal levees have been observed in the Dutch Wadden Sea during spring tides under extremely calm wave conditions. Observations show that they usually exist on a small scale (width < 50 m). Our work suggests that their spatial scale is related to the duration and magnitude of the forcing enhancing shoal

edge deposition. Their evolution occurs over multiple tidal cycles and only in extreme situations (limited wave action for days), they grow to extents which can be visually identified. In reality, the regular alternation between forcing inducing deposition and erosion (e.g., Geomor team, 1984) could limit their growth to visible extents. A continuously varying wave climate in nature could be the reason for levees being short-lived dynamic features and that we do not see them in most profiles. Cross Sections A7 and A8 (Figure 3) are located on a shoal that resembles our modeling configuration. Despite no visible levees being identified at the two survey moments, both cross sections showed bed-level changes with the highest changes being at the shoal seaward section.

More long-term high-resolution data are needed to further validate the co-relation between levees and wind-wave activity. The existence of such features could also be due to other forcing variations such as sediment supply or tidal range (e.g., spring/neap tides). Our work suggests that tidal levees are essential for explaining the shoal evolution since the processes leading to their formation/destruction represent the sediment balance at the shoal seaward edge. The reproduction of such features can be a good indication of the model's ability to capture the channel-shoal dynamics. This relatively short timescale dynamics are highly relevant for investigating the morphological impact of long-term forcing changes such as SLR.

6.2. SLR

We assumed equilibrium concentrations at the model boundaries which are maintained during SLR. However, in real scenarios, this may not be the case. Sediment needs to be available for import at the offshore boundary. The morphological response of other estuarine elements (e.g., channels or ebb-tidal delta) to SLR may lead to a change in prevailing SSC and sediment redistribution within the system which would eventually impact the sediment supply toward the shoals and limit the shoal accretion.

ASMITA is an example of a model that explicitly addresses these dynamics in an aggregated manner. The grid resolution covers entire entities such as the ebb-tidal delta, the basin's channel, and the basin's intertidal flats represented as volumes. An important assumption of this model is that equilibrium occurs when uniform concentrations exist within the system. Morphodynamic adaptation due to a forcing change (e.g., SLR) follows empirical equations that describe the sediment demand and availability along with the transport capacity for the different morphological elements. A new dynamic equilibrium state is reached when uniform concentrations are restored.

Our approach explicitly defines detailed processes while ASMITA is based on empirical equilibrium concepts, which makes it more straightforward and faster to use. Wave impact and intratidal dynamics are implicitly reflected by calibration coefficients. Both approaches aim to reduce tide-residual sediment transport gradients by morphodynamic adaptations. In that sense, they should lead to the same results. Here we qualitatively compare our approach and model results to ASMITA.

Van Goor et al. (2003) explored SLR adaptation of tidal basins including intertidal area. Their work suggests that a linear SLR will lead to a deeper profile that follows SLR at the same rate. Our model reproduces this "overdepth" (see Figures 12b and S3) as well. We found that the adaptation timescale required to create the constant "overdepth" profile is long (about 200 years for an 800 m profile when an abrupt linear SLR of 100 cm/century is imposed). Also, we show that the "overdepth" value varies across the profile because the profile slope becomes milder under SLR. ASMITA confirms these results showing the inertia of entire estuarine systems adapting to a change in linear SLR rate from 11 to 56 cm/century within 200–400 years depending on the system's size and the element under consideration. Both approaches show that SLR adaptation timescale may be long (~centuries). It is plausible that the "overdepth" has been reached for the Dutch conditions of more than a millennia of relatively constant linear SLR (Vermeersen et al., 2018). However, a future increase in the SLR rate can still pose a notable threat to the intertidal area.

Both our work and Van Goor et al. (2003) suggest the existence of a state at which SLR is too fast to have a stable "overdepth." In our model, this state occurs when the SLR-induced disturbances at the shoal edge ("levees") do not reach the landward shoal section and the flat disintegrates. Van Goor et al. (2003) highlight that this drowning state comprises high uncertainties as it highly depends on parameters defining the adaptation timescale. ASMITA describes the detailed transport and adaptation processes described in this paper (intratidally varying wave action and sediment concentration along the profile, changing profile shape) by tuning parameters such as a diffusion coefficient and fall velocity. These parameters do not represent

actual physical values but merely reflect representative processes. There is insufficient long-term field data to improve the parameters estimates. Future studies may focus on quantifying these parameters by our process-based approach.

6.3. Future Research

There is value in gradually increasing the model complexity by incorporating more processes such as 3-D processes, multiple sand fractions, and more detailed implementation of cohesive fractions including sand-mud interactions. A real case study implementation can provide validation of the research findings and a better connection to reality. This requires the acquisition of high temporal and spatial resolution long-term data with the focus on the channel-shoal dynamics.

Extending the study toward a large scale incorporating a part of or a whole estuary configuration is the next step. This extension would allow for investigating SLR impact on the different estuarine morphological elements along with their interactions and the impact of sediment supply. Also, it would enable exploring a variety of geometric shoal configurations such as a free shoal.

7. Conclusions

This study explores the mechanisms that drive the long-term morphological evolution of estuarine intertidal sandy shoals across a range of timescales. We developed a Delft3D, 2DH high-resolution, process-based model to simulate the morphological evolution of a channel-fringing shoal system inspired by conditions in the WS.

Observations and modeling studies in literature suggest that shoals aim to evolve toward a stable morphodynamic state maintained by a balance between sediment supply, wave action, and tidal forcing. Short-term morphological variations around the equilibrium occur in response to natural forcing variations such as wind-wave activity.

We investigated a shoal in morphodynamic equilibrium and its response to both short-term (wave action) and long-term (SLR) forcing changes. These disturbances result in a morphological adaptation that first impacts the shoal edge and gradually propagates landward. The area near the channel-shoal interface experiences the largest morphological adaptation. Tidal levees develop/erode at the shoal edge when wave action decreases/increases. The levees resemble observed features in estuaries (e.g., Western Scheldt) and tidal basins (e.g., Wadden Sea). A continuously varying wind-wave climate in nature can be the reason why they are dynamic and often short-lived features that are hard to capture in bathymetric surveys. Our work suggests that tidal levees are an essential part of the shoal evolution since their governing processes represent the sediment balance at the shoal edge. Such features should be taken into account when exploring the morphological response of shoals to long-term forcing variations such as SLR.

SLR has a long-term (approximately centuries) and a larger spatial-scale impact. The whole shoal accretes in response to SLR mainly due to the drop of wave-induced shear stress. However, accretion rates are less than the SLR rate due to inertia-induced phase lag (decades) between the bed-level response and SLR which is at its highest at the landward edge and at its lowest near the channel. Natural recovery from 100 years of SLR can range from decades to centuries depending on estuarine forcing conditions. Assuming the continuation of the current observed linear SLR showed larger accretion rates and a decreased lag compared to a sinusoidal rise, especially at landward locations. Accretion rates increased with time and reached the SLR rate after ≈200 years, suggesting that the profile reached a new deeper, milder slope, equilibrium state that follows SLR at the same rate with a temporally constant "overdepth." Incorporating mud fractions, it showed that shoals in a muddy environment could be more resilient against SLR. The mixture profile exhibited larger profile accretion due to increased mud deposition which made the shoal slightly muddier.

Shoals are quite resilient features in the sense that they are able to adapt to forcing changes without fundamentally changing their structure. However, a long (decades) lag is involved in the profile adaptation to SLR. In all SLR simulations, shoals experience a drop in intertidal area and increased inundation. In real scenarios, a possible shortage of sediment supply to shoals could amplify this effect. This raises questions about possible mitigation and adaptation measures to ensure the sustainability of the valuable intertidal environment.

Data Availability Statement

There is no restriction on the data used in this study. The readers can download the LIDAR and bathymetry data (source: Rijkwaterstaat). The reports used to construct Figure 1 and the numerical model configuration can be downloaded online at https://figshare.com/s/5f3d76060c39a5f437f8 (temporary link).

Acknowledgments
This study was partially funded by Deltares Research Funds. The modeling work was carried out on the Dutch national e-infrastructure with the support of SURF Cooperative. The authors highly appreciate the thoughtful comments by the five anonymous reviewers, which helped improve and focus the manuscript.

References

Adams, P. N., Slingerland, R. L., & Smith, N. D. (2004). Variations in natural levee morphology in anastomosed channel flood plain complexes. *Geomorphology*, *61*(1–2), 127–142. https://doi.org/10.1016/J.GEOMORPH.2003.10.005

Ahnert, F. (1960). Estuarine meanders in the Chesapeake Bay area. *Geographical Review*, *50*(3), 390–401. https://doi.org/10.2307/212282

Allen, J. R. L., & Duffy, M. J. (1998). Medium-term sedimentation on high intertidal mudflats and salt marshes in the Severn estuary, SW Britain: The role of wind and tide. *Marine Geology*, *150*(1–4), 1–27. https://doi.org/10.1016/S0025-3227(98)00051-6

Best, Ü. S. N., Van der Wegen, M., Dijkstra, J., Willemsen, P. W. J. M., Borsje, B. W., & Roelvink, D. J. A. (2018). Do salt marshes survive sea level rise? Modelling wave action, morphodynamics and vegetation dynamics. *Environmental Modelling & Software*, *109*, 152–166. https://doi.org/10.1016/J.ENVSOFT.2018.08.004

Braat, L., van Kessel, T., Leuven, J. R. F. W., & Kleinhans, M. G. (2017). Effects of mud supply on large-scale estuary morphology and development over centuries to millennia. *Earth Surface Dynamics*, *5*(4), 617–652. https://doi.org/10.5194/esurf-5-617-2017

Brierley, G. J., Ferguson, R. J., & Woolfe, K. J. (1997). What is a fluvial levee? *Sedimentary Geology*, *114*(1–4), 1–9. https://doi.org/10.1016/S0037-0738(97)00114-0

Carniello, L., Defina, A., Fagherazzi, S., & D'Alpaos, L. (2005). A combined wind wave-tidal model for the Venice lagoon, Italy. *Journal of Geophysical Research*, *110*, F04007. https://doi.org/10.1029/2004JF000232

Christie, M. C., Dyer, K. R., & Turner, P. (1999). Sediment flux and bed level measurements from a macro tidal mudflat. *Estuarine, Coastal and Shelf Science*, *49*(5), 667–688. https://doi.org/10.1006/ecss.1999.0525

Church, J. A., Clark, P. U., Cazenave, A., Gregory, J. M., Jevrejeva, S., Levermann, A., et al. (2013). Sea level change. In T. F. Stocker, D. Qin, G.-K. Plattner, M. Tignor, S. K. Allen, J. Boschung, A. Nauels, Y. Xia, V. Bex, & P. M. Midgley (Eds.), *Climate change 2013: The physical science basis. Contribution of Working Group I to the Fifth Assessment Report of the Intergovernmental Panel on Climate Change* (pp. 1137–1216). Cambridge, England: Cambridge University Press.

Cleveringa, J. (2013). *Ontwikkeling mesoschaal Westerschelde (factsheets)*. Antwerpen (in Dutch): International Marine & Dredging Consultants/Deltares/Svašek Hydraulics BV/ARCADIS Nederland BV. Retrieved from http://www.scheldemonitor.be/en/imis?module=ref&refid=232276

Coeveld, E. M., Hibma, A., & Stive, M. J. F. (2003). Feedback mechanisms in channel-shoal formation. In *Coastal sediments conference, St. Petersburg, FL, USA*. on CD-ROM(1–10). Texas, USA: World Scientific Publishing Corp, East meets West production.

Dam, G., van der Wegen, M., Labeur, R. J., & Roelvink, D. (2016). Modeling centuries of estuarine morphodynamics in the Western Scheldt estuary. *Geophysical Research Letters*, *43*, 3839–3847. https://doi.org/10.1002/2015GL066725

de Vet, L. (2020). *Intertidal flats in engineered estuaries: On the hydrodynamics, morphodynamics, and implications for ecology and system management*. Delft, The Netherlands: TU Delft. Retrieved from https://doi.org/10.4233/uuid:2b392951-3781-4aed-b093-547c70cc581d

Deltares. (2017). *Delft3D-FLOW: Simulation of multi-dimensional hydrodynamic flows and transports phenomena, including sediments. User Manual, Version 3.15, Revision 45038*, Delft, The Netherlands: Deltares.

Dissanayake, D. M. P. K., Ranasinghe, R., & Roelvink, J. A. (2009). Effect of sea level rise in tidal inlet evolution: A numerical modelling approach. *Journal of Coastal Research*, *2*, 942–946. Retrieved from http://www.jstor.org/stable/25737925

Elmilady, H., van der Wegen, M., Roelvink, D., & Jaffe, B. E. (2019). Intertidal area disappears under sea level rise: 250 years of morphodynamic modeling in San Pablo Bay, California. *Journal of Geophysical Research: Earth Surface*, *124*, 38–59. https://doi.org/10.1029/2018JF004857

Engelund, F., & Hansen, E. (1967). *A monograph on sediment transport in alluvial streams*. 0stervoldgade 10, Copenhagen K: Technical University of Denmark.

Fredsøe, J. (1984). Turbulent boundary layer in wave-current motion. *Journal of Hydraulic Engineering*, *110*(8), 1103–1120. https://doi.org/10.1061/(ASCE)0733-9429(1984)110:8(1103)

Friedrichs, C. (2011). Tidal flat morphodynamics. In *Treatise on estuarine and coastal science* (Vol. 3, pp. 137–170). Elsevier. https://doi.org/10.1016/B978-0-12-374711-2.00307-7

Friedrichs, C., & Aubrey, D. G. (1996). Uniform bottom shear stress and equilibrium hyposometry of intertidal flats. *Mixing in estuaries and coastal seas*, *Coastal and Estuarine Studies*. Washington, DC: American Geophysical Union. https://doi.org/10.1029/CE050p0405

Ganju, N. K., & Schoellhamer, D. H. (2010). Decadal-timescale estuarine geomorphic change under future scenarios of climate and sediment supply. *Estuaries and Coasts*, *33*(1), 15–29. https://doi.org/10.1007/s12237-009-9244-y

Ganju, N. K., Schoellhamer, D. H., & Jaffe, B. E. (2009). Hindcasting of decadal-timescale estuarine bathymetric change with a tidal-timescale model. *Journal of Geophysical Research*, *114*, F04019. https://doi.org/10.1029/2008JF001191

Geomor team (1984). *Geomorfologische processen Oosterschelde, een pilot study, Nota DDWT-84.006*. Netherlands (in Dutch): Rijkswaterstaat Dienst Getijdewateren. Retrieved from http://publicaties.minienm.nl/documenten/geomor-geomorfologische-processen-oosterschelde-een-pilot-study

Guo, L., van der Wegen, M., Roelvink, D., & He, Q. (2015). Exploration of the impact of seasonal river discharge variations on long-term estuarine morphodynamic behavior. *Coastal Engineering*, *95*, 105–116. https://doi.org/10.1016/j.coastaleng.2014.10.006

Guo, L. C. (2014). *Modeling estuarine morphodynamics under combined river and tidal forcing. PhD Thesis. UNESCO-IHE & Delft Technical University*. Delft, The Netherlands: CRC Press. Retrieved from https://www.crcpress.com/Modeling-Estuarine-Morphodynamics-under-Combined-River-and-Tidal-Forcing/Guo/p/book/9781138027503

Handleman, M. (2015). *Earth's rising seas*. Maryland, USA: NASA's Goddard Space Flight Center. Retrieved from https://svs.gsfc.nasa.gov/11927

Hibma, A. (2004). *Morphodynamic modeling of estuarine channel-shoal systems. Ph.D. thesis*. The Netherlands: Technical University Delft.

Hibma, A., de Vriend, H. J., & Stive, M. J. F. (2003). Numerical modelling of shoal pattern formation in well-mixed elongated estuaries. *Estuarine, Coastal and Shelf Science*, *57*(5–6), 981–991. https://doi.org/10.1016/S0272-7714(03)00004-0

Houser, C., & Hill, P. (2010). Wave attenuation across an intertidal sand flat: Implications for mudflat development. *Journal of Coastal Research*, *263*, 403–411. https://doi.org/10.2112/08-1117.1

Hu, Z., Wang, Z. B., Zitman, T. J., Stive, M. J. F., & Bouma, T. J. (2015). Predicting long-term and short-term tidal flat morphodynamics using a dynamic equilibrium theory. *Journal of Geophysical Research: Earth Surface*, *120*, 1803–1823. https://doi.org/10.1002/2015JF003486

Jaffe, B. E., Smith, R. E., & Foxgrover, A. C. (2007). Anthropogenic influence on sedimentation and intertidal mudflat change in San Pablo Bay, California: 1856-1983. *Estuarine, Coastal and Shelf Science*, *73*(1–2), 175–187. https://doi.org/10.1016/j.ecss.2007.02.017

Janssen-Stelder, B. (2000). The effect of different hydrodynamic conditions on the morphodynamics of a tidal mudflat in the Dutch Wadden Sea. *Continental Shelf Research*, *20*(12-13), 1461–1478. https://doi.org/10.1016/S0278-4343(00)00032-7

Kemp, A. C., Horton, B. P., Donnelly, J. P., Mann, M. E., Vermeer, M., & Rahmstorf, S. (2011). Climate related sea-level variations over the past two millennia. *Proceedings of the National Academy of Sciences*, *108*(27), 11,017–11,022. https://doi.org/10.1073/pnas.1015619108

Kohsiek, L. H. M., Buist, H. J., Misdorp, R., Berg, J. H., & Visser, J. (1988). Sedimentary processes on a Sandy shoal in a Mesotidal estuary (Oosterschelde, the Netherlands). In *Tide-influenced sedimentary environments and facies* (pp. 201–214). Dordrecht, The Netherlands: Reidel. https://doi.org/10.1007/978-94-015-7762-5_16

Lesser, G. R., Roelvink, D., van Kester, J. A. T. M., & Stelling, G. S. (2004). Development and validation of a three-dimensional morphological model. *Coastal Engineering*, *51*(8–9), 883–915. https://doi.org/10.1016/j.coastaleng.2004.07.014

Leuven, J., de Haas, T., Braat, L., & Kleinhans, M. G. (2018). Topographic forcing of tidal sandbar patterns for irregular estuary planforms. *Earth Surface Processes and Landforms*, *43*(1), 172–186. https://doi.org/10.1002/esp.4166

Leuven, J., Kleinhans, M., Weisscher, S. A. H., & van der Vegt, M. (2016). Tidal sand bar dimensions and shapes in estuaries. *Earth-Science Reviews*, *161*, 204–223. https://doi.org/10.1016/j.earscirev.2016.08.004

Lipcius, R. N., Seitz, R. D., Wennhage, H., Bergström, U., & Ysebaert, T. (2013). Ecological value of coastal habitats for commercially and ecologically important species. *ICES Journal of Marine Science*, *71*(3), 648–665. https://doi.org/10.1093/icesjms/fst152

Luan, H. L., Ding, P. X., Wang, Z. B., & Ge, J. Z. (2017). Process-based morphodynamic modeling of the Yangtze estuary at a decadal timescale: Controls on estuarine evolution and future trends. *Geomorphology*, *290*, 347–364. https://doi.org/10.1016/J.GEOMORPH.2017.04.016

Luan, H. L., Ding, P. X., Wang, Z. B., Ge, J. Z., & Yang, S. L. (2016). Decadal morphological evolution of the Yangtze estuary in response to river input changes and estuarine engineering projects. *Geomorphology*, *265*, 12–23. https://doi.org/10.1016/J.GEOMORPH.2016.04.022

Maan, D. C., van Prooijen, B. C., Wang, Z. B., & De Vriend, H. J. (2015). Do intertidal flats ever reach equilibrium? *Journal of Geophysical Research: Earth Surface*, *120*, 2406–2436. https://doi.org/10.1002/2014JF003311

Maan, D. C., van Prooijen, B. C., Zhu, Q., & Wang, Z. B. (2018). Morphodynamic feedback loops control stable fringing flats. *Journal of Geophysical Research: Earth Surface*, *123*, 2993–3012. https://doi.org/10.1029/2018JF004659

Narayan, S., Beck, M. W., Wilson, P., Thomas, C. J., Guerrero, A., Shepard, C. C., et al. (2017). The value of coastal wetlands for flood damage reduction in the northeastern USA. *Scientific Reports*, *7*(1), 9463. https://doi.org/10.1038/s41598-017-09269-z

NASA (2019). *Sea Level*. Maryland, USA: NASA Goddard Space Flight Center. https://climate.nasa.gov/vital-signs/sea-level/

Normark, W. R., Piper, D. J. W., Posamentier, H., Pirmez, C., & Migeon, S. (2002). Variability in form and growth of sediment waves on turbidite channel levees. *Marine Geology*, *192*(1–3), 23–58. https://doi.org/10.1016/S0025-3227(02)00548-0

Parris, A., Bromirski, P., Burkett, V., Cayan, D., Culver, M., Hall, J., et al. (2012). *Global sea level rise scenarios for the US National Climate Assessment*. Silver Spring, Maryland: NOAA Tech Memo OAR CPO-1 NOAA. https://scenarios.globalchange.gov/sites/default/files/NOAA_SLR_r3_0.pdf

Partheniades, E. (1965). Erosion and deposition of cohesive soils. *Journal of the Hydraulics Division*, *91*(1), 105–139.

Perillo, G. M. E., & Iribarne, O. O. (2003). Processes of tidal channel development in salt and freshwater marshes. *Earth Surface Processes and Landforms*, *28*(13), 1473–1482. https://doi.org/10.1002/esp.1018

Pritchard, D., & Hogg, A. J. (2003). Cross-shore sediment transport and the equilibrium morphology of mudflats under tidal currents. *Journal of Geophysical Research*, *108*(C10), 3313. https://doi.org/10.1029/2002JC001570

Pritchard, D., Hogg, A. J., & Roberts, W. (2002). Morphological modelling of intertidal mudflats: The role of cross-shore tidal currents. *Continental Shelf Research*, *22*(11–13), 1887–1895. https://doi.org/10.1016/S0278-4343(02)00044-4

Ranasinghe, R., Wu, C. S., Conallin, J., Duong, T. M., & Anthony, E. J. (2019). Disentangling the relative impacts of climate change and human activities on fluvial sediment supply to the coast by the world's large rivers: Pearl River Basin, China. *Scientific Reports*, *9*(1), 9236. https://doi.org/10.1038/s41598-019-45442-2

Ridderinkhof, H., Van der Ham, R., & Van der Lee, W. (2000). Temporal variations in concentration and transport of suspended sediments in a channel-flat system in the ems-Dollard estuary. *Continental Shelf Research*, *20*(12–13), 1479–1493. https://doi.org/10.1016/S0278-4343(00)00033-9

Roberts, W., Le Hir, P., & Whitehouse, R. J. (2000). Investigation using simple mathematical models of the effect of tidal currents and waves on the profile shape of intertidal mudflats. *Continental Shelf Research*, *20*(10–11), 1079–1097. https://doi.org/10.1016/S0278-4343(00)00013-3

Roelvink, J. A. (1993). Dissipation in random wave groups incident on a beach. *Coastal Engineering*, *19*(1–2), 127–150. https://doi.org/10.1016/0378-3839(93)90021-Y

Roelvink, J. A. (2006). Coastal morphodynamic evolution techniques. *Coastal Engineering*, *53*(2–3), 277–287. https://doi.org/10.1016/j.coastaleng.2005.10.015

Rossington, K., & Spearman, J. (2009). Past and future evolution in the Thames estuary. *Ocean Dynamics*, *59*(5), 709–718. https://doi.org/10.1007/s10236-009-0207-4

Schramkowski, G. P., Schuttelaars, H. M., & de Swart, H. E. (2002). The effect of geometry and bottom friction on local bed forms in a tidal embayment. *Continental Shelf Research*, *22*(11–13), 1821–1833. https://doi.org/10.1016/S0278-4343(02)00040-7

Seminara, G., & Tubino, M. (2001). Sand bars in tidal channels. Part 1. Free bars. *Journal of Fluid Mechanics*, *440*, 49–74. https://doi.org/10.1017/S0022112001004748

Shepard, C. C., Crain, C. M., & Beck, M. W. (2011). The protective role of coastal marshes: A systematic review and meta-analysis. *PLoS ONE*, *6*(11), e27374. https://doi.org/10.1371/journal.pone.0027374

Straub, K. M., & Mohrig, D. (2008). Quantifying the morphology and growth of levees in aggrading submarine channels. *Journal of Geophysical Research*, *113*, F03012. https://doi.org/10.1029/2007JF000896

Temmerman, S., Bouma, T. J., Govers, G., Wang, Z. B., De Vries, M. B., & Herman, P. M. J. (2005). Impact of vegetation on flow routing and sedimentation patterns: Three-dimensional modeling for a tidal marsh. *Journal of Geophysical Research*, *110*, F04019. https://doi.org/10.1029/2005JF000301

Thatcher, M. L., & Harleman, D. R. F. (1972). *Prediction of unsteady salinity intrusion in estuaries: Mathematical model and user's manual*. Cambridge, Massachusetts: S. G. P. O. Massachusetts Institute of Technology & N. S. G. P. (U.S.). Retrieved from https://repository.library.noaa.gov/view/noaa/9602

van der Wegen, M. (2013). Numerical modeling of the impact of sea level rise on tidal basin morphodynamics. *Journal of Geophysical Research: Earth Surface*, *118*, 447–460. https://doi.org/10.1002/jgrf.20034

van der Wegen, M., Jaffe, B., Foxgrover, A., & Roelvink, D. (2017). Mudflat morphodynamics and the impact of sea level rise in South San Francisco Bay. *Estuaries and Coasts*, *40*(1), 37–49. https://doi.org/10.1007/s12237-016-0129-6

van der Wegen, M., Jaffe, B. E., & Roelvink, J. A. (2011). Process–based, morphodynamic hindcast of decadal deposition patterns in San Pablo Bay, California, 1856–1887. *Journal of Geophysical Research*, *116*, F02008. http://doi.org/10.1029/2009JF001614

van der Wegen, M., & Roelvink, D. (2008). Long-term morphodynamic evolution of a tidal embayment using a two-dimensional, process-based model. *Journal of Geophysical Research*, *113*, C03016. https://doi.org/10.1029/2006JC003983

van der Wegen, M., & Roelvink, D. (2012). Reproduction of estuarine bathymetry by means of a process-based model: Western Scheldt case study, the Netherlands. *Geomorphology*, *179*, 152–167. https://doi.org/10.1016/j.geomorph.2012.08.007

van der Wegen, M., Roelvink, J. A., & Jaffe, B. E. (2019). Morphodynamic resilience of intertidal mudflats on a seasonal time scale. *Journal of Geophysical Research: Oceans*, *124*, 8290–8308. https://doi.org/10.1029/2019JC015492

van der Wegen, M., Wang, Z. B., Savenije, H. H. G., & Roelvink, J. A. (2008). Long-term morphodynamic evolution and energy dissipation in a coastal plain, tidal embayment. *Journal of Geophysical Research*, *113*, F03001. https://doi.org/10.1029/2007JF000898

Van Goor, M. A., Zitman, T. J., Wang, Z. B., & Stive, M. J. F. (2003). Impact of sea-level rise on the morphological equilibrium state of tidal inlets. *Marine Geology*, *202*(3–4), 211–227. https://doi.org/10.1016/S0025-3227(03)00262-7

van Maanen, B., Coco, G., Bryan, K. R., & Friedrichs, C. T. (2013). Modeling the morphodynamic response of tidal embayments to sea-level rise. *Ocean Dynamics*, *63*(11-12), 1249–1262. https://doi.org/10.1007/s10236-013-0649-6

Van Rijn, L. C. (1993). *Principles of sediment transport in rivers, estuaries and coastal seas*. Amsterdam, The Netherlands: Aqua publications.

van Veen, J., van der Spek, A. J. F., Stive, M. J. F., & Zitman, T. (2005). Ebb and flood channel systems in the Netherlands tidal waters. *Journal of Coastal Research*, *216*, 1107–1120. https://doi.org/10.2112/04-0394.1

van Vessem, P. (1984a). *Selectie meetdagen behoeve van Comor, Hiswa en Doos2. Nota WWKZ-84G.284*. Netherlands: Rijkswaterstaat. (in Dutch)

van Vessem, P. (1984b). *Selectie meetdagen behoeve van Comor, Hiswa en Doos2. Nota WWKZ-84G.293*. Netherlands: Rijkswaterstaat. (in Dutch)

Vermeersen, B. L. A., Slangen, A. B. A., Gerkema, T., Baart, F., Cohen, K. M., Dangendorf, S., et al. (2018). Sea-level change in the Dutch Wadden Sea. *Netherlands Journal of Geosciences*, *97*(3), 79–127. https://doi.org/10.1017/njg.2018.7

Wang, Z. B., Elias, E. P. L., van der Spek, A. J. F., & Lodder, Q. J. (2018). Sediment budget and morphological development of the Dutch Wadden Sea: Impact of accelerated sea-level rise and subsidence until 2100. *Netherlands Journal of Geosciences*, *97*(3), 183–214. https://doi.org/10.1017/njg.2018.8

Yang, S.-L., Friedrichs, C. T., Shi, Z., Ding, P.-X., Zhu, J., & Zhao, Q.-Y. (2003). Morphological response of tidal marshes, flats and channels of the outer Yangtze River mouth to a major storm. *Estuaries*, *26*(6), 1416–1425. https://doi.org/10.1007/BF02803650

Zhou, X., Zheng, J., Doong, D.-J., & Demirbilek, Z. (2013). Sea level rise along the East Asia and Chinese coasts and its role on the morphodynamic response of the Yangtze River estuary. *Ocean Engineering*, *71*, 40–50. https://doi.org/10.1016/J.OCEANENG.2013.03.014

Zhou, Z., Coco, G., Townend, I., Olabarrieta, M., Van Der Wegen, M., Gong, Z., et al. (2017). Is "morphodynamic equilibrium" an oxymoron? *Earth-Science Reviews*, *165*, 257–267. https://doi.org/10.1016/j.earscirev.2016.12.002

Zhou, Z., Coco, G., van der Wegen, M., Gong, Z., Zhang, C., & Townend, I. (2015). Modeling sorting dynamics of cohesive and non-cohesive sediments on intertidal flats under the effect of tides and wind waves. *Continental Shelf Research*, *104*, 76–91. https://doi.org/10.1016/J.CSR.2015.05.010

Zhou, Z., Ye, Q., & Coco, G. (2016). A one-dimensional biomorphodynamic model of tidal flats: Sediment sorting, marsh distribution, and carbon accumulation under sea level rise. *Advances in Water Resources*, *93*, 288–302. https://doi.org/10.1016/J.ADVWATRES.2015.10.011

Zhu, Q., van Prooijen, B. C., Wang, Z. B., & Yang, S. L. (2017). Bed-level changes on intertidal wetland in response to waves and tides: A case study from the Yangtze River Delta. *Marine Geology*, *385*, 160–172. https://doi.org/10.1016/j.margeo.2017.01.003